X-ray Scattering Study of Tl Adlayers on the Au(111) Electrode in Alkaline Solutions: Metal Monolayer, OH- Coadsorption, and Oxide Formation

ARTICLE *in* THE JOURNAL OF PHYSICAL CHEMISTRY · JULY 1994

Impact Factor: 2.78 · DOI: 10.1021/j100080a014

3 AUTHORS, INCLUDING:

Jia Wang
Brookhaven National Laboratory
106 PUBLICATIONS **4,692** CITATIONS

X-ray Scattering Study of Tl Adlayers on the Au(111) Electrode in Alkaline Solutions: Metal Monolayer, OH^- Coadsorption, and Oxide Formation

J. X. Wang,*,† R. R. Adzic,† and B. M. Ocko‡

Department of Applied Science, Chemical Sciences Division, and Department of Physics, Brookhaven National Laboratory, Upton, New York 11973

Received: February 22, 1994®

The structure of electrodeposited Tl adlayers on Au(111) in 0.1 M NaOH has been investigated using surface X-ray scattering. Incommensurate, hexagonal Tl structures exist over a wide potential region positive of bulk deposition. In the potential region between -0.66 and -0.38 V (versus Ag/AgCl), the Tl monolayer is rotated from the substrate axes by 5.2°-6.2° and is closely packed with a Tl-Tl separation ranging from 3.34 to 3.43 Å. Between -0.36 and -0.18 V, an incommensurate, aligned-hexagonal phase is observed in which the Tl-Tl spacing increases with increasing potential from 3.88 to 4.10 Å. The first-order transformation between these two phases at -0.37 V involves the coadsorption of OH^-. For the aligned-hexagonal phase the electrosorption valence is larger than unity, which indicates that partially-charged hydroxyl species are coadsorbed. The coadsorption of OH^- facilitates the existence of this unusual low-coverage, incommensurate Tl phase. At more positive potentials, the hexagonal adlayer lattice continuously rotates away from the substrate axes. At $E >$ -0.04 V the adlayer appears disordered, and a two Tl atom thick Tl_2O adlayer forms. The data illustrate the power of the surface X-ray scattering techniques, coupled with electrochemical measurements, in studying the complex behavior of electrodeposited adlayers.

1. Introduction

Underpotential deposition (UPD) refers to the electrodeposition of metals at potentials positive of the Nernst potential. It occurs when the adatom-substrate bonding is stronger than the adatom-adatom bonding in the bulk phase.[1] On single crystal electrode surfaces, the UPD processes often exhibit voltammetry features which are correlated with the formation of well-ordered adlayer structures. It is now possible to determine the structure of these UPD adlayers by *in situ* surface X-ray scattering (SXS), scanning tunneling microscopy (STM), and atomic force microscopy (AFM) techniques (see e.g. refs 2-9). An important finding of all of these studies is that the nearest-neighbor separation of the deposited metal layer—at potentials close to the bulk deposition potential—is always very close to the bulk interatomic spacings. These close-packed structures are similar to the structures formed by vapor deposition in vacuum. In contrast, for UPD adlayers formed at more positive potentials, the nearest-neighbor separations are much larger than the bulk values.[7,8] These open structures often exhibit pronounced electrocatalytic effects[10] and may be technologically relevant.

In this paper we report the first *in situ* structural study of UPD adlayers in alkaline solution. The results reveal the effects of OH^- adsorption on the structures and chemical states of three out of four Tl adlayer structures at the Au(111) electrode. For instance, over a range of potentials OH^- is coadsorbed with the Tl, and together they form an incommensurate monolayer where the Tl-Tl separation is much larger than the bulk value. The existence of OH^- coadsorption, in the present study, has also been confirmed by the measured electrosorption valence and X-ray specular reflectivity. The phase transition between this coadsorbed phase and the close-packed Tl monolayer phase is discontinuous. In the voltammetry curve, the corresponding current spikes support the notion of a first-order phase transition. Furthermore, the transition potential corresponds to the potential where the oxygen reduction switches from a two-electron to a four-electron process.[11] These features, all of which occur at the same potential, demonstrate the relationship between surface structure and electrochemical reactivity.

At potentials negative to the bulk Tl^+/Tl^{3+} redox reaction, the voltammetry shows a surface oxidation peak which has been attributed to the formation of a thallium oxide monolayer.[11,12] Prior to the present study, there have been no reported *in situ* structural measurements of these UPD metal oxide adlayers. From the X-ray specular reflectivity analysis, we show that a two Tl adatom thick Tl_2O adlayer forms on the Au(111) surface. In addition, the monovalent nature of the Tl in the oxide layer has been deduced from the charge associated with the oxidation process and from the Tl coverages before and after oxidation. The surface uniformity has been confirmed by STM studies.[13]

2. Experimental Aspects

A gold disk (2-mm by 10-mm diameter) was aligned and polished as previously reported.[14] The angle between the optical plane and the [111] crystallographic plane was measured to be 0.15°. After sputtering and annealing in a vacuum chamber, the sample was transferred through air into an electrochemical X-ray scattering cell constructed from Kel-F.[14] The cell was sealed using a 4-μm-thick Prolene (Chemplex Inc.) X-ray window. The solutions were prepared from TlF (Johnson Matthey) or $TlNO_3$ (Aldrich), NaOH solution (Fisher), $HClO_4$ (Merck), and Milipore QC water (Milipore Inc.) and were deoxygenated. An outer cell was filled with flowing nitrogen gas to prevent oxygen diffusing through the Prolene film during the measurements. At a potential slightly positive of the bulk Tl deposition potential, the cell was deflated, which leaves a thin (~10-μm-thick) electrolyte film between the Au(111) face and the X-ray window. A Ag/AgCl (3 M KCl) electrode was used as a reference electrode. In order to minimize the chloride leakage to the cell, the reference electrode was separated by two frits with 0.1 M NaOH solution between them.

SXS measurements were carried out at the National Synchrotron Light Source (NSLS) at beam line X22B with $\lambda = 1.54$ Å (in-plane diffraction) and at beam line X22C with $\lambda = 1.24$ Å (specular reflectivity). A full description of the electrochemical

* To whom correspondence should be addressed.
† Department of Applied Science, Chemical Sciences Division.
‡ Department of Physics.
® Abstract published in *Advance ACS Abstracts*, June 15, 1994.

0022-3654/94/2098-7182$04.50/0

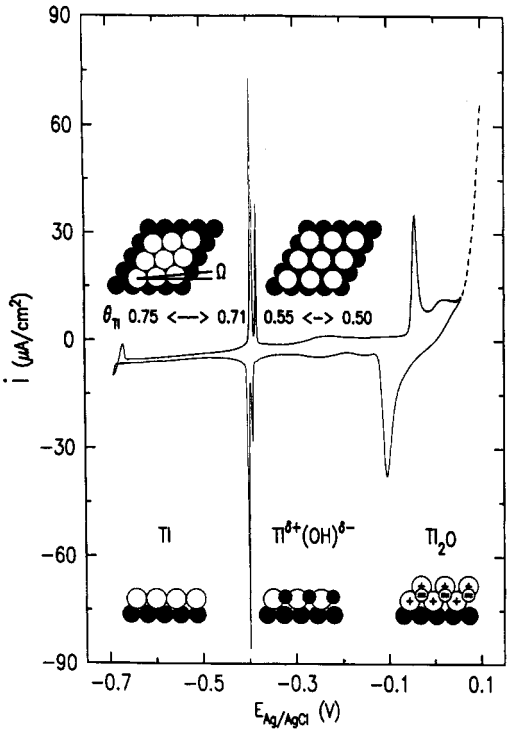

Figure 1. Linear sweep voltammogram obtained at 5 mV/s for Tl UPD on Au(111) in 0.1 M NaOH with 5 mM TlF. The in-plane structural models of the Tl monolayer and the Tl coverages were obtained from grazing incident angle diffraction measurements. The chemical compositions and surface normal structure models were derived from X-ray specular reflectivity, in-plane diffraction, and electrochemical data (see text).

SXS technique has been presented elsewhere.[14] For in-plane diffraction measurements, the q-space resolution within the scattering plane was determined primarily by the Soller slits on the detector arm. This arrangement provides a 2θ resolution of 0.1° half-width at half-maximum (hwhm), which corresponds to a longitudinal in-plane resolution of 0.007-Å^{-1} hwhm. The transverse in-plane resolution was limited by the mosaic spread of the gold crystal which is about 0.05° hwhm. For Au(111) it is convenient to use a hexagonal coordinate system in which a position in reciprocal space is given by $(a^*,b^*,c^*)\cdot(H,K,L)$, where $a^* = b^* = 4\pi/\sqrt{3}a = 2.52$ Å^{-1}, $c^* = 2\pi/\sqrt{6}a = 0.89$ Å^{-1}, and $a = 2.885$ Å. The in-plane diffraction measurements were carried out in the (H,K) plane with $L = 0.2$ corresponding to a grazing angle of 1.25°.

3. Voltammetry of Tl Adlayers and Its Structural Implications

The linear potential sweep voltammetry curve for the UPD of Tl on Au(111) in 0.1 M NaOH containing 5 mM TlF is shown in Figure 1. At the reversible Nernst potential for bulk Tl deposition in this solution (–0.67 V), a pair of peaks is observed which represents the onset of the bulk Tl deposition and dissolution. A large increase in the anodic current at $E > 0.1$ V is due to the onset of the Tl^+/Tl^{3+} reaction (dashed line). The Nernst potentials for the formation of $Tl(OH)_3$ and Tl_2O_3 in this solution are –0.03 and 0.11 V, respectively.[15] In the potential region between these limits, the UPD of Tl takes place, as indicated by the current spikes at ~–0.4 V and the peaks at ~–0.1 V. The considerable double-layer charging current in the potential region between –0.38 and –0.1 V is indicative of a surface reaction involving partially charged species, while the small current in the potential region negative to –0.4 V indicates that the neutral species are present on the surface. The oxidation of the Au(111) surface occurs above 0.1 V in 0.1 M NaOH.[16] Consequently, these X-ray scattering studies were carried out between –0.66 and 0.0 V.

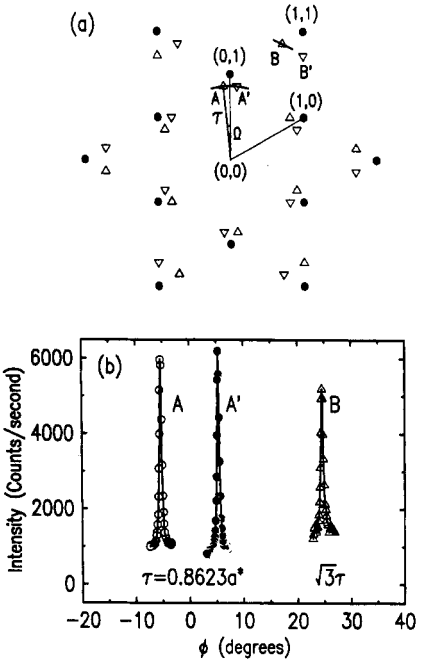

Figure 2. (a) In-plane diffraction patterns for Au(111)/Tl at –0.7 V in 0.1 M NaOH with 0.5 mM TlF. The solid circles represent the diffraction pattern from the Au(111) substrate. The triangles and inverted triangles represent the diffraction patterns from the Tl monolayer in the two symmetry-equivalent domains of the rotated-hexagonal phase. (b) Azimuthal scans through the position A, A', and B as indicated in (a). For clarity, the diffraction intensity in the scan through position B has been multiplied by factor 10.

The charges associated with the anodic current peaks at –0.38, –0.36, and –0.04 V in the voltammetry shown in Figure 1 are 33, 13, and 80 μC/cm^2, respectively. Assuming a one-electron exchange, these charges correspond to 0.15, 0.06, and 0.36 monolayers since 220 μC/cm^2 is required for the oxidation of one monolayer on Au(111). These peaks, however, are not due to a simple stripping of Tl adatoms since they depend on both the Tl^+ concentration and solution pH. In addition, disc-ring measurements indicate that, upon oxidation of Tl near –0.04 V, the Tl adatoms do not leave the Au surface; rather, more Tl^+ is adsorbed on the surface.[12] Based on the electrosorption valency of Tl adsorbates and the X-ray diffraction data, the current spike at –0.36 V is interpreted in terms of the coadsorption of OH^- ions which leads to the formation of the aligned-hexagonal phase. The structural models and coverages for the different Tl adlayers shown in Figure 1 are deduced from the SXS measurements discussed in the following sections.

4. In-Plane Surface Structure

A. High-Coverage Rotated-Hexagonal Phase. Grazing incident angle X-ray diffraction measurements were performed in order to determine the surface structure of electrodeposited thallium adlayers. In the absence of Tl adsorption, the in-plane diffraction pattern from the unreconstructed Au(111) surface is composed of only the integer reflections which are shown as solid circles in Figure 2a.[14] The presence of an electrodeposited Tl adlayer at –0.7 V in 0.1 M NaOH with 0.5 mM TlF gives rise to additional diffraction features which are shown by the triangles and inverted triangles. This pattern corresponds to the diffraction from the two symmetry equivalent domains of an incommensurate, hexagonally close-packed Tl monolayer. The angle Ω represents the angle by which the diffraction pattern is rotated from the low-index gold reflections. The symmetric pair of reflections closest to (0,1) is labeled as A and A' in the figure. At the lowest-order hexagonal peak the magnitude of the in-plane wave vector, $|Q_\parallel|$, gives the Tl reciprocal space constant, τ. Since the Tl lattice is

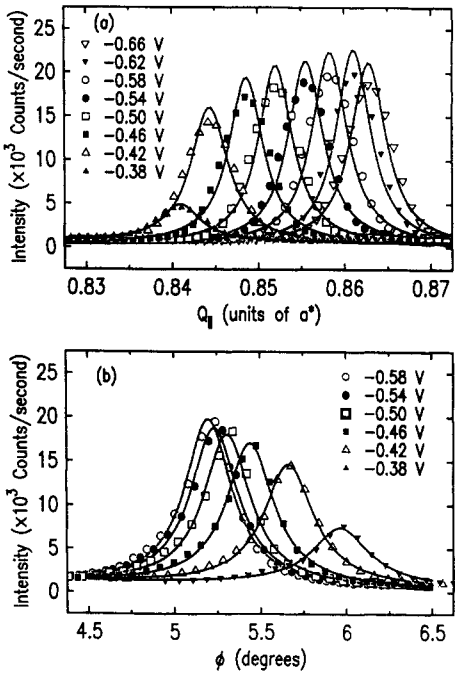

Figure 3. Radial scans (a) and azimuthal scans (b) through one of the low-order diffraction peaks of the Tl monolayer in the high-coverage, rotated-hexagonal phase at different potentials in 0.1 M NaOH with 5 mM TlF. The solid lines are the fits to the Lorentzian line shape. In the azimuthal scans $\phi = 0$ corresponds to the <01> axis.

hexagonal, the real space lattice constant $a_{Tl} = 4\pi/\tau\sqrt{3}$. At −0.7 V, in a 0.1 M NaOH solution with 0.5 mM TlF, $\tau = 0.8623a^*$. This corresponds to a Tl nearest-neighbor separation, $a_{Tl} = 3.35$ Å. Since the normalized Tl coverage, θ, is equal to $(a/a_{Tl})^2 = (\tau/a^*)^2$, the coverage at this potential is 0.742 Tl atom for every gold surface atom. In Figure 2b azimuthal scans (ϕ scans) through A, A', and B are shown. For A and A', the magnitude of the in-plane wave vector was kept at τ in the scan. The diffraction peaks are symmetrically centered at ±5.1° from the <0,1> direction. For $|Q_\parallel| = \sqrt{3}\tau$, the diffraction peak is located at 24.9°, which is exactly 30° from peak A. Radial scans through this peak (not shown) are accurately centered at $|Q_\parallel| = \sqrt{3}\tau$. Thus, the observed diffraction pattern demonstrates that the Tl adlayer is a rotated-hexagonal phase. The same diffraction pattern has been observed for Pb and Tl on the Ag(111)[2,5] and for I on the Au(111)[17] electrode surfaces.

In order to study the phase behavior in the rotated-hexagonal phase, the potential dependence for one of the low-order diffraction peaks was followed after each step change in potential. Equilibrium was typically achieved in 5 min. In-plane radial and azimuthal scans were carried out to respectively determine the Tl lattice constant and the rotation angle. In Figure 3a the radial scans, acquired in 0.1 M NaOH containing 5 mM TlF, are shown between −0.66 and −0.38 V in increments of 0.04 V. At all potentials the diffraction peaks are well described by Lorentzian profiles (solid lines). The peak shifts to smaller $Q_\parallel$ as the potential increases which corresponds to a decrease in the coverage. The diffracted intensity decreases with increasing potential as the coverage decreases. The only exception to this trend is the most negative potential of −0.66 V. Since this potential is close to the Nernst potential for bulk Tl deposition (−0.67 V), the slight decrease of the diffracted intensity at −0.66 V is likely due to the onset of bulk deposition. At −0.38 V the intensity was significantly diminished, and by −0.36 V the diffraction from the rotated-hexagonal phase vanished.

Subsequent to each radial scan shown in Figure 3a, an azimuthal scan was taken with $|Q_\parallel| = \tau$. As shown in Figure 3b, a well-defined diffraction maximum was observed at all potentials. The peak position (defined as Ω) shifts to larger angles as the potential

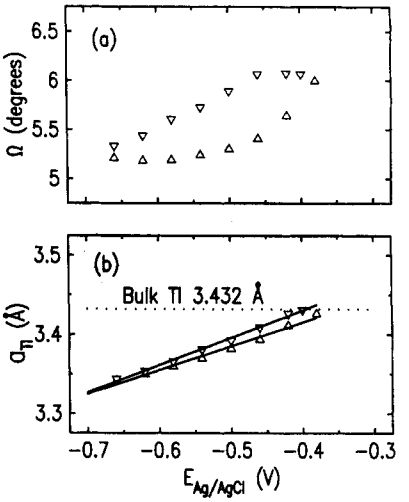

Figure 4. Rotation angle (a) and hexagonal lattice constant (b) of the Tl monolayer on Au(111) in 0.1 M NaOH with 5 mM TlF as a function of potential in positive (triangles) and negative (inverted triangles) sweeping directions. The solid lines in (b) are linear fits to the data.

increases. Between −0.66 and −0.50 V, Ω is nearly independent of potential and has a value of 5.25 ± 0.1°. Above −0.46 V Ω increases, and at −0.38 V it has a value of 6.1°. These azimuthal diffraction scans have been fit to Lorentzian profiles in order to accurately obtain the rotation angle and the angular peak width. The Lorentzian profile (solid lines in Figure 3b) provides an excellent description of the data at all potentials. The rotation angle determined from these fits as a function of potential is shown in Figure 4a. The data exhibit significant hysteresis between the two sweep directions. Similar effects have been observed for Tl on Ag(111).[5] Below −0.42 V the fitted Lorentzian width is 0.17°. This corresponds to a transverse width in reciprocal space of $\tau \sin(0.17°) = 0.00625$ Å^{-1}. The inverse transverse width (e.g., 1/0.00625 Å^{-1} = 160 Å), without the corrections for the spectrometer resolution function and for the sample mosaic, provides a measure of the coherence length of the Tl adlayer.

The radial peak position provides an accurate measure of $\tau(E)$. In Figure 4b, a_{Tl}, calculated from $\tau(E)$, is plotted versus the potential for both positive and negative potential sweeps. The figure shows that a_{Tl} measured in the positive sweep (triangles) is slightly smaller than the values obtained in the negative sweep (inverted triangles). The rotated-hexagonal Tl monolayer formed at the most positive potential of −0.38 V has $a_{Tl} = 3.43$ Å. This is exactly the average nearest-neighbor spacing for bulk Tl.[18] At −0.66 V, which is the most negative potential where the monolayer Tl phase exists, $a_{Tl} = 3.34$ Å. This corresponds to a compression of 2.6% when compared to the bulk Tl spacing, and this finding is in agreement with results of Toney and co-workers[19] obtained in neutral solutions. The agreement is expected since OH^- anions do not adsorb at the surface below −0.40 V at pH ≤ 13. The potential dependence of a_{Tl} can be fitted to a linear form for both the positive and negative sweeps, and the results of these fits are displayed as solid lines in Figure 4b. The slopes in the linear fits are 0.303 and 0.346 Å/V for the positive and negative potential sweeps, respectively. These values are only slightly larger than the values obtained for Tl monolayer on Ag(111).[5] It is worth noting, however, that the Tl monolayer is only stable up to $a_{Tl} = 3.38$ Å on Ag(111), whereas it is observed up to $a_{Tl} = 3.43$ Å on Au(111). Whereas a Tl bilayer forms on Ag(111) just prior to bulk deposition, no such phase is observed on Au(111).

The epitaxy of incommensurate, hexagonal monolayers has been studied theoretically by Novaco and McTague.[20] In their model, the free energy is minimized with respect to the angle of rotation of the adlayer at a fixed incommensurability. On this basis, they predict that the rotation angle at zero temperature should depend on the incommensurability in a linear manner and

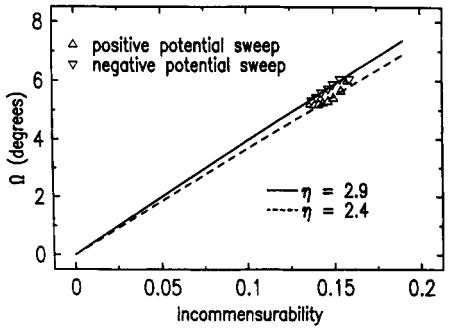

Figure 5. Rotation angle of the Tl monolayer lattice with respect to the Au(111) substrate axis as a function of the incommensurability. The solid and dashed lines show the values predicted by Novaco–McTague theory[20] with η = 2.9 and 2.4, respectively.

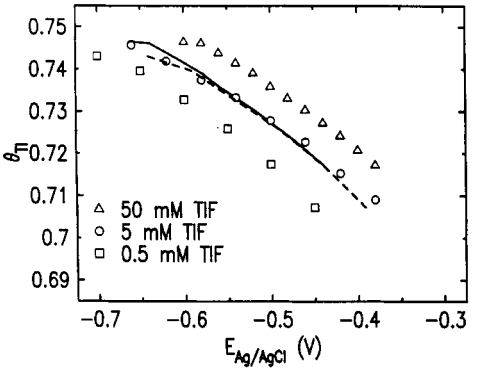

Figure 6. Tl coverage on Au(111) in the high-coverage, rotated-hexagonal phase as a function of potential in 0.1 M NaOH with different TlF concentrations. The solid and dashed lines show the 50 and 0.5 mM data shifted by –0.059 and 0.059 V, respectively.

that the apparent slope depends on the ratio of elastic constants. This model qualitatively describes the phase behavior of adsorbates on graphite,[20,21] Tl electrodeposited on Ag(111)[5] and I on Au(111).[17] In Figure 5, the rotation angle of the Tl monolayer is plotted against the incommensurability, $1 - \tau/a^*$. The solid and dashed lines show the calculated values obtained from the Novaco–McTague model with η equal to 2.9 and 2.4, respectively. Within the contexts of the model, $\eta \equiv (C_L/C_T)^2 - 1$, where C_L and C_T are the monolayer longitudinal and transverse sound velocities. Previously, η has been estimated to be 2.75 for Tl monolayer.[5] As shown in Figure 5, the data agree with the Novaco–McTauge model for $2.4 < \eta < 2.9$. The effect of the sweep direction on the rotation angle is not understood at present.

Additional SXS measurements were carried out with different Tl^+ concentrations in order to determine the electrosorption valence. In Figure 6, the potential dependence of the Tl coverage, calculated from measured lattice constants, is shown for 0.1 M NaOH containing 0.5, 5, and 50 mM Tl. For all three concentrations the coverage decreases in a linear manner with increasing potential. The primary effect of the concentration is to shift the coverage–potential curves positively by 0.059 V for each decade increase of Tl^+ concentration. This is illustrated by the solid and dashed lines which show the 50 and 0.5 mM data shifted by –0.059 and 0.059 V, respectively (Figure 6). Both lines fall on the data obtained in 5 mM TlF solution.

The electrosorption valence, γ, has been obtained from Figure 6. It describes the potential dependence of the electrosorption equilibria and can be used to estimate the charge transferred between the electrode and the adsorbate. According to Shultze and Vetter,[22] in the case of a concentrated supporting electrolyte, the electrosorption valence for adsorbed species is given by

$$\gamma = \frac{-1}{F}\left(\frac{\partial Q_m}{\partial \Gamma_{ad}}\right)_E = \frac{1}{F}\left(\frac{\partial \mu_s}{\partial E}\right)_{\Gamma_{ad}} \qquad (1)$$

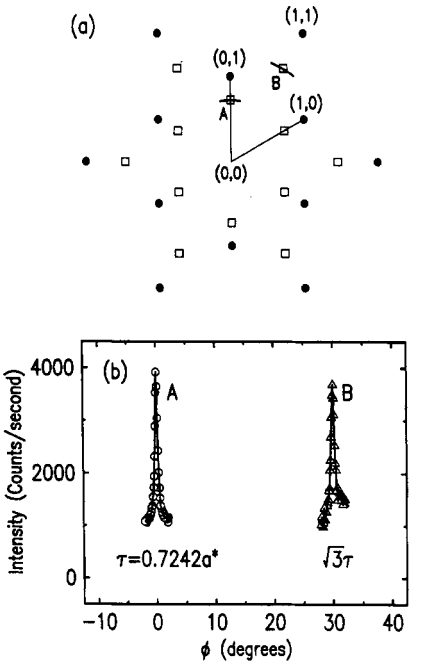

Figure 7. (a) In-plane diffraction patterns for Au(111)/Tl at –0.3 V in 0.1 M NaOH with 0.5 mM TlF. The solid circles represent the diffraction pattern from the Au(111) substrate. The squares represent the diffraction pattern from the Tl monolayer in the aligned-hexagonal phase. (b) Azimuthal scans through the positions *A* and *B* as indicated in (a). For clarity, the diffraction intensity in the scan through position *B* has been multiplied by a factor 10.

where F is Faraday constant, μ_s is the chemical potential of the reactant in the electrolyte solution, E is the electrode potential, Q_m is the charge on the metal electrode, and Γ_{ad} is the surface concentration of adsorbed species. From eq 1, γ can be determined from the potential dependence of the adsorption equilibrium at constant Γ_{ad}, i.e.

$$\gamma = \frac{RT}{F}\left(\frac{\partial \ln a_s}{\partial E}\right)_{\Gamma_{ad}} = 0.059\left(\frac{\partial \log a_s}{\partial E}\right)_{\Gamma_{ad}} \qquad (2)$$

where R is the molar gas constant, T is temperature, a_s is the activity of the reactant in the solution, and $RT\ln(10)/F = 0.059$ V for room temperature. For small concentration of Tl^+, the activity can be approximated by the concentration. With this approximation, the application of eq 2 to the data shown in Figure 6 yields $\gamma \simeq 1$ for adsorbed Tl. This implies that the Tl adatoms are neutral in the high-coverage rotated-hexagonal phase.

B. Aligned-Hexagonal Phase. At potentials positive of the rotated-hexagonal phase potential regime, the Tl adlayer forms an incommensurate, aligned-hexagonal phase at the Au(111) surface. As shown in Figure 7a, all of the diffraction peaks from the adlayer are aligned along the Au(111) axes. Therefore, we refer to this phase as an aligned-hexagonal phase. Typical azimuthal scans at $|Q_\parallel| = \tau$ and $|Q_\parallel| = \sqrt{3}\tau$ are shown in Figure 7b.

Figure 8 displays radial and azimuthal scans in the aligned-hexagonal phase in a 0.1 M NaOH solution with 5 mM Tl^+ between –0.36 and –0.2 V. When the aligned-hexagonal phase first appears at –0.36 V, the radial scan is centered at $|Q_\parallel| = 0.743a^*$ (see Figure 8a), which corresponds to a coverage of 0.552. As the potential is increased, the diffraction maximum shifts to lower $|Q_\parallel|$, and at –0.20 V the peak is centered to $0.703a^*$ corresponding to a coverage of 0.494. The decrease of diffracted intensity with potential in the range from –0.36 to –0.24 V can be understood in terms of the expected quadratic scattering intensity dependence on the electron density (i.e., coverage). Above –0.24 V, the change in the scattered intensity with increasing

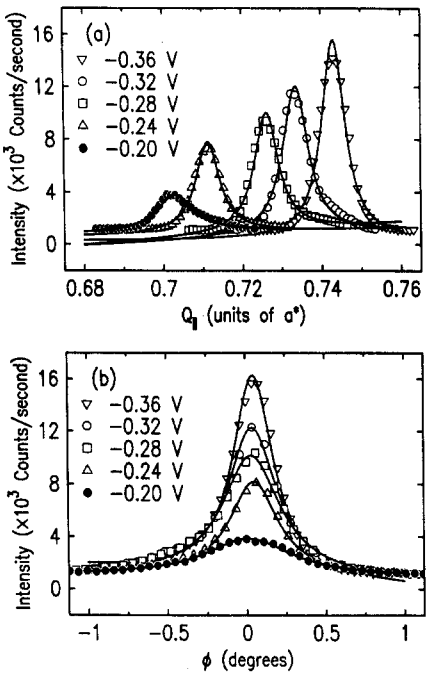

Figure 8. Radial scans (a) and azimuthal scans (b) through one of the low-order diffraction peaks of the Tl monolayer in the aligned-hexagonal phase at different potentials in 0.1 M NaOH with 5 mM TlF. The solid lines are the fits to the Lorentzian line shape. In the azimuthal scans ϕ = 0 corresponds to the <01> axis.

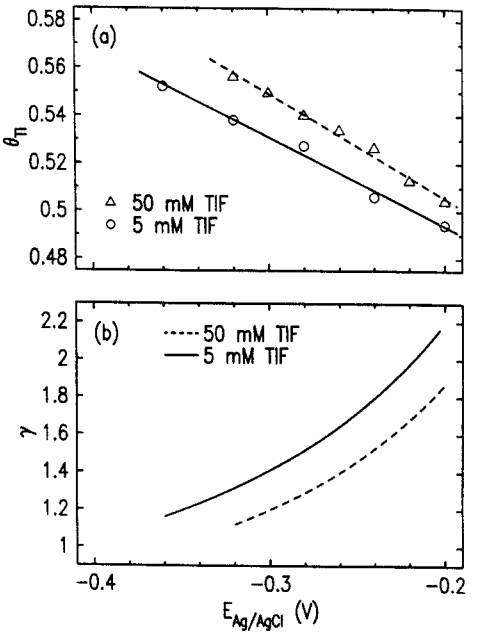

Figure 9. (a) Tl coverage on Au(111) in the aligned-hexagonal phase as a function of potential in 0.1 M NaOH with 50 mM TlF (triangles) and 5 mM TlF (circles). The solid and dashed lines are the linear fits to the data. (b) Electrosorption valence calculated from the data in (a) by applying eq 2.

potential deviates from the quadratic form. This deviation may indicate another phase transition.

Concurrent with the radial scans, the azimuthal scans were recorded at each potential. Typical azimuthal scans shown in Figure 8b indicate that the profiles are peaked at $\Phi = 0°$ at potentials between –0.36 and –0.20 V. The Lorentzian fits, shown as solid lines, adequately describe the aligned-hexagonal phase. Although the average fitted azimuthal hwhm of 0.19° is slightly larger than the 0.17° in the rotated-hexagonal phase, the transverse coherence length remains the same (160 Å) since τ is smaller.

Assuming one Tl atom per unit cell, the Tl coverage in the aligned-hexagonal phase was obtained using the peak positions in the radial scans shown in Figure 8a. The same measurements were carried out in 50 mM TlF. The effect of Tl^+ concentration on the coverage–potential curve is shown in Figure 9a. The solid lines are the linear fits to the data. By applying eq 2 to the linear fits shown in Figure 9a, the potential-dependent electrosorption valence is obtained (see Figure 9b). That the values of γ are larger than one in this potential region indicates that the partially-discharged OH^- species are coadsorbed in the aligned-hexagonal phase. This is because γ cannot exceed 1 for the electrosorption of Tl^+. The existence of charged adsorbates at the surface can be inferred from the voltammetry curve (cf. Figure 1), in which the double-layer charging current is considerably larger at potentials above –0.36 V than that at more negative potentials where only neutral Tl atoms are adsorbed. As expected, this aligned-hexagonal phase does not exist in acid solution due to a lack of OH^- ions.[23] The fact that γ increases with increasing *potential* suggests that more OH^- ions are adsorbed at higher potentials. The hydroxyl species may adsorb within or on top of the Tl monolayer. This is consistent with the X-ray specular reflectivity results (section 5). It is, however, difficult to determine the exact coverage and position of adsorbed OH^-.

C. Low-Coverage Rotated-Hexagonal Phase. At potentials positive of –0.2 V (0.1 M NaOH with 5 mM TlF) the aligned-hexagonal adlayer undergoes a continuous transition to a low-coverage rotated-hexagonal adlayer. This transition is first apparent from the broadening in the azimuthal profiles. At more

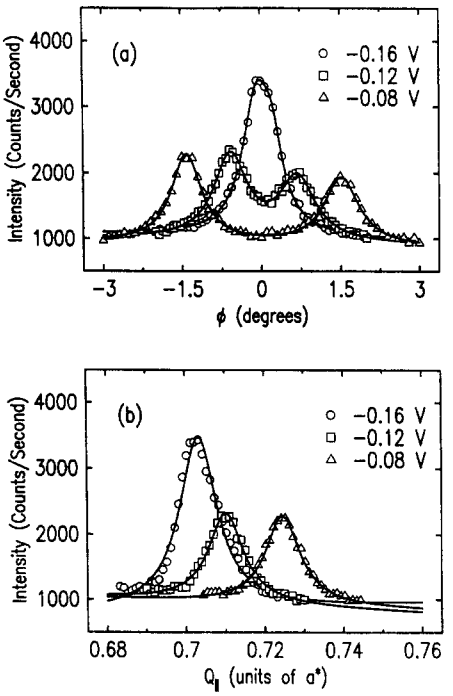

Figure 10. Azimuthal scans (a) and radial scans (b) through one of the low-order diffraction peak of the Tl monolayer in the low-coverage, rotated-hexagonal phase at different potentials in 0.1 M NaOH with 5 mM TlF. The solid lines are the fits to the sum of two Lorentzian profiles in (a) and to a single Lorentzian line shape in (b). In the azimuthal scans ϕ = 0 corresponds to the <01> axis.

positive potentials, two well-defined peaks emerge in the azimuthal scan which are symmetrically arranged about the principal gold reflections. Azimuthal scans at –0.16 (circles), –0.12 (squares), and –0.08 V (triangles) are shown in Figure 10a along with associated Lorentzian fits (solid lines). At –0.16 V, the single Lorentzian fitted profile hwhm is 0.37°, which is significantly broader than that in the aligned-hexagonal phase. At potential above –0.1 V, the azimuthal scans exhibit a well-defined pair of peaks. This "split peak" is reminiscent of the high-coverage rotated-hexagonal phase observed at more negative potentials

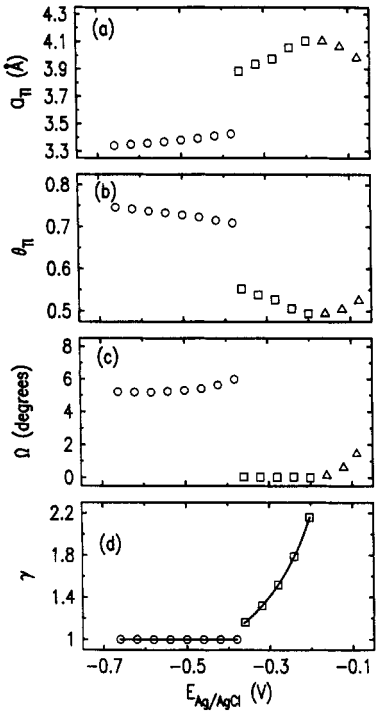

Figure 11. Hexagonal lattice constant (a), coverage (b), rotation angle (c), and electrosorption valence (d) of the Tl monolayer in 0.1 M NaOH with 5 mM TlF as a function of potential incremented by 0.04 V. The circles, squares, and triangles represent the high-coverage, rotated-hexagonal phase, the aligned-hexagonal phase, and the low-coverage, rotated-hexagonal phase, respectively.

(see Figure 2b). As the potential is further increased, the splittings increases, corresponding to an increase in the rotation angle.

In conjunction with the azimuthal measurements described above, radial scans (see Figure 10b) were also taken in the low-coverage rotated-hexagonal phase. At –0.16 V (circles), the peak is centered at $0.703a^*$ ($\theta = 0.495$), while at –0.08 V (triangles) the peak is centered at $0.725a^*$ ($\theta = 0.525$). Since the coverage increases above –0.16 V and below –0.20 V, it is clear that the coverage reaches a minimum at about –0.18 V. The increase in coverage with increasing potential above –0.18 V suggests the onset of a new surface process.

The low-coverage rotated-hexagonal phase is not stable above –0.04 V. After about 30 min at –0.04 V the scattered intensity completely vanished. This is probably due to the process associated with the anodic current peak at the same potential (Figure 1). Subsequent to the disappearance of the low-coverage phase, the diffraction data were acquired while stepping the potential in the negative direction. The diffraction intensity slowly recovered with decreasing potential from –0.08 to –0.16 V. Both the lattice constant and rotation angle did not, however, vary with potential during the measurements. Above –0.04 V, no in-plane diffraction from an adlayer was observed.

D. Phase Behavior of Tl Monolayer Phases. The data presented in the previous three subsections are summarized in Figure 11. In 0.1 M NaOH containing 5 mM TlF, the Tl adlayer forms incommensurate, hexagonal phases on Au(111) over a 0.6-V-wide potential range. The hexagonal lattice constant (a), coverage (b), rotation angle (c), and the electrosorption valence (d) are displayed for the three phases as a function of potential in Figure 11. Discontinuities in these variables indicate phase transitions. Within each phase, the continuous change of the lattice constant is consistent with the incommensurate nature of the monolayer.

A nearly reversible phase transition occurs at –0.37 V between the high-coverage, rotated-hexagonal phase and the aligned-hexagonal phase. In the positive potential sweep, this phase transition is accompanied by a discontinuous increase of a_{Tl} from 3.43 to 3.88 Å (Figure 11a). The latter value is 13% larger than the bulk Tl–Tl spacing. The formation of such a low-coverage, yet incommensurate, phase is attributed to the coadsorption of OH^-. As discussed in section 4B, that the electrosorption valence is larger than one in the aligned-hexagonal phase indicates that partially-charged hydroxyl species are coadsorbed (Figure 11d). The coverage change associated with the phase transition, calculated from the in-plane diffraction measurements, is 0.16 (0.71–0.55) of a monolayer as shown in Figure 11b. This coverage change is very close to the 0.15 monolayer obtained by integrating the charge associated with the first anodic current peak at –0.38 V (see Figure 1). The second anodic current peak at –0.36 V appears to be connected with the surface rearrangement of Tl adatoms with simultaneous adsorption of the OH^- ions. It results in the formation of the aligned-hexagonal Tl phase with coadsorbed OH^-. This is supported by the appearance of the new phase at the same potential as the voltammetry peak. In addition, this assignment is supported by the fact that this current peak does not appear in acidic solutions where the aligned-hexagonal phase does not exist.

The transition from the aligned-hexagonal to the low-coverage rotated-hexagonal phase involves a continuous rotation of the Tl lattice away from the substrate axes and a decrease of the hexagonal lattice constant with increasing potential. For this phase, the Tl coverage calculated from the lattice constant starts to increase with increasing potential. Since the OH^- adsorption increases with increasing potential, the oxidation of Tl adatoms at potentials above –0.18 V does not result in the desorption of Tl adatoms into the solution phase,[11] but rather the formation of thallium oxide takes place at the surface. This conclusion is supported by the reflectivity data discussed in the next section. The low-coverage rotated-hexagonal phase is a precursor to the disordered Tl oxide adlayer.

5. Surface Normal Structure: X-ray Reflectivity

As previously demonstrated,[14,24] the absolute X-ray specular reflectivity, $R(L)$, is sensitive to the surface normal electron density profile at an electrode/electrolyte interface. In order to ascertain the surface normal structure of the Tl adlayer phases, X-ray specular reflectivity measurements were carried out in the high-coverage rotated-hexagonal phase, in the aligned-hexagonal phase, and in the oxide adlayer phase. The Tl coverage at these potentials, obtained from analysis of the reflectivity profiles, confirms that the Tl adlayer in the hexagonal phases is a monolayer and reveals the existence of the two Tl atom thick oxide adlayer.

Figure 12 shows the absolute specular reflectivity, $R(L)$, between $L = 0.20$ and 6.5 in the high-coverage rotated-hexagonal phase at –0.62 V (circles), in the low-coverage aligned-hexagonal phase at –0.35 V (squares), and in the oxide adlayer phase at –0.05 V (triangles) along with several model curves. The principal features of the reflectivity spectra are the Bragg peaks at L equal to 3 and 6 corresponding to the cubic (111) and (222) reflections and the much weaker, potential-dependent reflectivity at intermediate wave vectors. At all three potentials the measured reflectivity deviates from the calculated reflectivity for the ideally terminated Au(111) crystal which is shown as the dashed curve. The solid lines are the results of fits to simple real space models which are described below.

The reflectivity from the Au(111) surface, $R(L)$, can be expressed in terms of a sum over atomic layers, $s(Q_z)$,[25]

$$R(L) = \left|\frac{256\pi^2 r_0^2}{3a^2 Q_z^2}\right| |T(\alpha)|^4 \, e^{L_{abs}/\sin(\alpha)} |s(Q_z)|^2 \qquad (3)$$

where r_0 is the Thomson radius of the electron, α is the incident angle, $Q_z = 2\pi L/c$, and $|T(\alpha)|^4$ is related to the enhancement of the electric field at the surface. The absorption of the thin layer

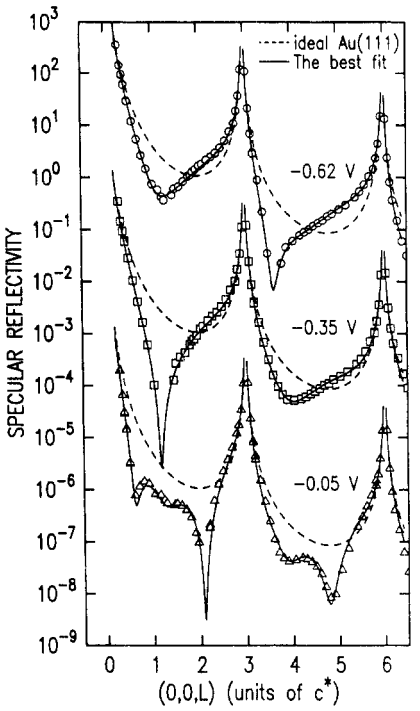

Figure 12. Specular reflectivity from Au(111) in 5 mM TlF + 0.1 M NaOH at –0.62 V (circles), –0.35 V (squares), and –0.05 V (triangles). The dotted line shows the reflectivity from an ideally terminated Au(111) surface. The solid lines are the best fits using the models discussed in the text.

electrolyte is significant at small incident angle and the absorption constant, $L_{abs} \simeq 0.015$, is obtained from the fits.

The sum over atomic layers of gold and thallium can be written as

$$s(Q_z) = \sum_{m=1}^{3} F_{Tl}(Q_z)\theta_m e^{-Q_z^2\sigma_m^2/2}e^{-iQ_z d_m} + F_{Au}(Q_z)(e^{-Q_z^2\sigma_0^2/2}e^{-iQ_z d_0} + e^{-Q_z^2\sigma_B^2/2}\sum_{n=0}^{\infty} e^{iQ_z nd}) \quad (4)$$

which incorporates up to three Tl atomic layers, one non-ideally-terminated Au layer, and an infinite sum over ideally-terminated gold layers.[26] The atomic form factors of gold and thallium are given by $F_{Au}(Q_z)$ and $F_{Tl}(Q_z)$. For the mth Tl layer θ_m is the coverage, σ_m is the root-mean-square (rms) atomic displacement along the surface normal direction, and d_m is the distance between the mth layer and topmost, ideally-terminated gold layer. For the non-ideally-terminated gold layer, σ_0 is the rms atomic displacement along the surface normal direction and d_0 is the distance between the layer and topmost ideally-terminated gold layer. At room tempertures the ideally-terminated gold layers are described by the bulk Debye–Waller factor, $\sigma_B = 0.085$ Å, and the gold layer spacing, $d = c/3$.

For the data obtained at –0.62 V (circles), the best fit, shown as the solid line in Figure 12, was obtained with only one Tl adlayer, e.g., $\theta_2 = \theta_3 = 0$, and a nonideal topmost gold layer. The parameters obtained from the fit are summarized in Table 1. The top gold layer was found to be slightly expanded, with $d_0 = 2.39$ Å which is 1.7% larger than the bulk gold interlayer spacing of 2.35 Å. This small top layer expansion has also been observed for electrodeposited metal layers and for electrodeposited iodine adlayers.[4,17] The Tl coverage, $\theta_1 = 0.72 \pm 0.02$, is close to the coverage of 0.74 calculated from the in-plane lattice parameters at this same potential. Adding an additional Tl monolayer to the fitting procedure did not significantly improve the quality of the fit, and the resulting coverage of this Tl layer is only 0.02.

TABLE 1: Parameters Obtained from Analysis of Specular Reflectivity Data

E (V)	atom	coverage	spacing[a] (Å)	rms (Å)
–0.62	Au	1.00	2.39 ± 0.02	0.11 ± 0.02
	Tl	0.72 ± 0.02	2.66 ± 0.02	0.18 ± 0.02
–0.35	Au	1.00	2.38 ± 0.02	0.10 ± 0.02
	Tl	0.61 ± 0.05	2.69 ± 0.02	0.36 ± 0.03
	Tl	0.05 ± 0.02	3.07 ± 0.09	0.28 ± 0.11
–0.05	Tl	0.56 ± 0.02	2.49 ± 0.02	0.21 ± 0.02
	Tl	0.49 ± 0.02	2.53 ± 0.02	0.32 ± 0.02
	Tl	0.18 ± 0.02	2.80 ± 0.04	0.32 ± 0.04

[a] The spacing corresponds to the separation between the referred layer and the underlying layer.

Therefore, we conclude that the high-coverage rotated-hexagonal phase is only composed of a single Tl layer. The layer spacing between the Tl monolayer and the top gold layer ($d_1 - d_0$) is 2.66 Å, which is close to the estimated distance of 2.62 Å. This estimate is made by assuming that the Au–Tl bonding length is the sum of the gold radius ($a/2 = 1.44$ Å) and the Tl covalent radius (1.48 Å). With these values, the Tl–Au layer spacings for Tl residing in atop sites, in bridging sites, and in hollow sites are 2.92, 2.54, and 2.40 Å, respectively. Since the Tl adlayer is incommensurate with the substrate, we calculate a layer spacing of 2.62 Å by averaging the spacings for all three sites. This suggests that there is a strong chemical bond between Au and Tl monolayer, since the covalent radius of Tl (1.48 Å) is much smaller than half of the nearest-neighbor spacing of bulk Tl (3.43/2 = 1.72 Å).

At –0.35 V, in the aligned-hexagonal phase, the reflectivity exhibits a deep minimum at a position between the origin and the first Bragg peak. This strong destructive interference results from the Tl coverage being close to half.[24] The best-fit curve (solids line) describes the essential feature of the data (squares) in Figure 12. As shown in Table 1, the top gold layer is slightly expanded as at –0.62 V, and the Au–Tl spacing of 2.69 Å is almost identical to the distance obtained in the high-coverage rotated-hexagonal phase. However, the Tl coverage in the first adlayer ($\theta_1 = 0.61$) is higher than the 0.55 coverage obtained from the in-plane measurement. In addition, there is a small Tl coverage present in the second adlayer ($\theta_2 = 0.05$).

The reflectivity model, as described by eqs 3 and 4, does not account for the effect of OH^- on the reflectivity spectrum. We can, however, interpret the effect of OH^- by considering the relative scattering amplitude between Tl and OH^-. Since the scattering amplitude is proportional to the electron density and since the ratio $Z_e(Tl)/Z_e(OH^-)$ is ~8, the 0.06 Tl monolayer difference in coverage between the values obtained from the reflectivity analysis and the in-plane diffraction can be attributed to about 0.5 monolayer of adsorbed-hydroxyl species. In this approximation, we have neglected the small L-dependent form factor difference between Tl and OH^-. Similarly, the 0.05 of a Tl monolayer in the second layer can be attributed to either a layer of hydroxyl species or an adsorbed layer of water.[14] Although the exact amount and position of the hydroxyl species cannot be determined from the above analysis, their existence at the surface is supported by the reflectivity analysis.

We have also carried out reflectivity studies in the thallium oxide phase. Within this phase the Tl coverage cannot be determined from the grazing incident angle diffraction measurements since no additional diffraction features beyond the gold pattern are observed. The surface normal structure of the oxide adlayer is crucial for understanding the complex oxidation process of the Tl adatoms. In order to completely oxidize the Tl adlayer, the system was equilibrated at 0.0 V for 5 min before stepping the potential to –0.05 V. This latter potential was chosen in order to avoid the oxidation of Tl^+ to Tl^{3+} and the reduction of thallium oxide. The reflectivity spectrum obtained at this potential (Figure 12) exhibits a double minimum between the Bragg positions whereas only a single minimum is observed at the other

two potentials. In analogy with the n-slit diffraction problem in ordinary optics, this second minimum suggests that at this potential an additional Tl layer was adsorbed on the surface with about the same coverage as the first Tl adlayer.

In the analysis the reflectivity at –0.05 V was first fitted to a model with a single, non-ideally-terminated Au layer and with two Tl layers. This model failed to describe the reflectivity at small L. The addition of a third Tl layer, albeit with a small density, significantly improved the quality of the fit within this region. To minimize the number of adjustable parameters, the small modification of the top gold layer was neglected. The best fit obtained with this model is shown by the solid line at the bottom of Figure 12. The Tl coverages obtained from the fit are $\theta_1 = 0.56$, $\theta_2 = 0.49$, and $\theta_3 = 0.18$. The layer spacing between the top gold layer and the first Tl layer is 2.49 Å, which is slightly smaller than in the hexagonal phases. The layer spacings between the first and second Tl layer and between the second and third layer are 2.54 and 2.80 Å, respectively. The rms displacement amplitudes are 0.22, 0.32, and 0.30 Å for the first, second, and third layer, respectively.

From the electron density profile derived above, and with the additional information obtained from the electrochemical and in-plane diffraction measurements, a simple picture of the thallium oxide surface layer emerges. Here, the Tl^+ atoms reside in two distinct layers which are separated by 2.54 Å, and the O^{2-} resides between these two layers, as shown in Figure 1. We will account for the oxygen by assuming that the excess coverages (e.g., the difference between the fitted coverage, $\theta_2 = 0.56$, and 0.5) is due to the oxygen. Specifically, the excess Tl coverage of 0.06 corresponds to about a 0.5 monolayer of O^{2-}. Because of the interaction of these anions with the positively charged electrode, it is possible that the O^{2-} shifts from the idealized center position between the two Tl^+ layers toward the gold surface. In the electron density profile, therefore, the density of the O^{2-} species are mixed with the density of the first Tl^+ layer. The 0.18 coverage in the third layer might result from additional OH^- adsorption and a small coverage of loosely bonded TlOH. The average, lateral Tl^+–Tl^+ spacing in the Tl_2O layer can be obtained from the coverage assuming an in-plane hexagonal arrangement of the Tl species. For a coverage of 0.5, it gives 4.08 Å. The nearest-neighbor separation of Tl^+ of 3.46 Å is calculated from the layer spacing (2.54 Å) and in-plane spacing (4.08 Å) by assuming that Tl^+ ions in the second layer are in the hollow sites of the first layer. These values indicate that the Tl_2O adlayer is a densely-packed adlayer which covers the surface in a uniform manner, in agreement with the STM imaging.[13]

The monovalence of Tl species in the oxide adlayer is deduced from the fact that the charge associated with the oxidation process at –0.04 V (Figure 1) is about 80 $\mu C/cm^2$. This is much less than the charge of ~440 $\mu C/cm^2$ required for formation of two half-monolayers of Tl^{3+}-containing species. According to the free enthalpy in bulk phase,[15] TlOH should be more stable than Tl_2O, but the data seem to suggest that the surface adlayer is a thallium oxide rather than thallium hydroxide. The Nernst potential for the oxidation of TlOH to $Tl(OH)_3$ is –0.09 V in 0.1 M NaOH, which is significantly lower than –0.04 V, the potential of the adlayer formation. Since anhydrous oxide (Tl_2O) requires a more positive potential for further oxidation than TlOH,[15] the potential of –0.04 V favors the formation of Tl_2O. From a structural point of view, the formation of a two Tl atom thick adlayer is also more likely than the two layers of TlOH because of the short layer spacing (2.54 Å) between the two layers. The in-plane diffraction data show that about 0.5 monolayer of $Tl^{\delta+}OH^{\delta-}$ is adsorbed on the surface at –0.1 V. Upon the oxidation of Tl adsorbates at the surface, another 0.5 monolayer of Tl^+ species is adsorbed to form the second atomic layer through a strong chemical bonding (2.54-Å layer spacing) with the first Tl layer. This unusual adsorbate-oxidation-induced adsorption of Tl^+ from the solution has been previously reported on the basis of ring-disc measurements[11] and now can be interpreted as the formation of Tl_2O.

6. Conclusions

The UPD of Tl on Au(111) in alkaline solution appears to be a system with exceptionally complex behavior. Several phenomena, usually not observed in the UPD of a single metal, *viz.*, coadsorption of OH^- anions, formation of a low-coverage incommensurate phase, sharp first-order transition between two incommensurate phases, and adsorption of an oxide monolayer, have been observed. By combining SXS and electrochemical techniques, the Tl adlayer structure, coverage, and electrosorption valence have been determined over a wide potential region. Three distinct chemical states of Tl adatoms have been identified in the potential region between bulk metal deposition and bulk Tl^+/Tl^{3+} oxidation. Prior to the bulk metal deposition, completely discharged Tl adatoms form an incommensurate, rotated-hexagonal monolayer. The Tl–Tl separation in this phase varies with potential from 3.43 (bulk value) to 3.34 Å. The rotation angle between the adlayer and the substrate agrees with the value predicted by the Novaco–McTauge model. These properties of the Tl monolayer are corroborated by the unity value of the electrosorption valence of Tl adatoms. In the intermediate potential region a new phenomenon, the OH^- coadsorption-induced ordering of Tl adatoms, has been observed. It gives rise to the formation of an incommensurate, aligned-hexagonal phase with the Tl–Tl separation varying with potential between 3.88 and 4.10 Å. That the potential-dependent electrosorption valence is larger than one for this phase is signifcant since it indicates the coadsorption of partially discharged OH^-. This facilitates the formation of an incommensurate phase of Tl with the Tl–Tl separation considerably larger than the bulk value. The stabilizing effect of the OH^- coadsorption warrants further studies with other metal adatoms. A determination of the structure and composition of the Tl_2O adlayer, which eluded previous efforts, was possible with a combination of X-ray reflectivity and electrochemical data. At the most positive potentials, a two Tl atom thick Tl_2O adlayer is formed which appears to have no long-range order within the surface plane. The Tl oxidation state was determined from the charge measured in voltammetry and the coverages obtained from X-ray scattering measurements before and after Tl surface oxidation. These results illustrate the exceptional power of SXS techniques, when combined with electrochemical methods, in determining the structural and oxidation states of metal adsorbates.

Acknowledgment. The authors thank W. Polewska, O. M. Magnussen, and S. Feldberg for helpful discussions. This research was performed under the auspices of the U.S. Department of Energy, Divisions of Chemical and Materials Sciences, Office of Basic Energy Sciences, under Contract DE-AC02-76CH00016.

References and Notes

(1) Kolb, D. M. In *Advances in Electrochemistry and Electrochemical Engineering*; Gerischer, H., Tobias, C. W., Eds.; Wiley-Interscience: New York, 1978; Vol. 11, pp 125–271.

(2) Melroy, O. R.; Toney, M. F.; Borges, G. L.; Samant, M. G.; Kortright, J. B.; Ross, P. N.; Blum, L. *Phys. Rev. B* **1988**, *38*, 10962.

(3) Toney, M. F.; Gordon, J. G.; Samant, M. G.; Borges, G. L.; Wiesler, D. G.; Yee, D.; Sorensen, L. B. *Langmuir* **1991**, *7*, 796.

(4) Adzic, R. R.; Wang, J.; Vitus, C. M.; Ocko, B. M. *Surf. Sci. Lett.* **1993**, *293*, 876.

(5) (a) Toney, M. F.; Gordon, J. G.; Kau, L.; Borges, G. L.; Melroy, O. R.; Samant, M. H.; Wiesler, D.; Yee, D.; Sorensen, L. *Phys. Rev. B* **1990**, *42*, 5594. (b) Toney, M. F.; Gordon, J. G.; Samant, M. H.; Borges, G. L.; Melroy, O. R.; Yee, D.; Sorensen, L. B. *Phys. Rev. B* **1992**, *45*, 9362.

(6) Chen, C.-H.; Kepler, K. D.; Gewirth, A. A.; Ocko, B. M.; Wang, J. *J. Phys. Chem.* **1993**, *97*, 7290.

(7) (a) Magnussen, O. M.; Hotlos, J.; Beitel, G.; Kolb, D. M.; Behm, R. J. *J. Vac. Sci. Technol. B* **1991**, *9*, 969. (b) Magnussen, O. M.; Hotlos, J.; Nichols, R. J.; Kolb, D. M.; Behm, R. J. *Phys. Rev. Lett.* **1990**, *64*, 2929. (c) Manne, S.; Hansma, P. K.; Massie, J.; Elings, V. B.; Gewirth, A. A. *Science* **1991**, *251*, 183.

(8) Chen, C.-H.; Gewirth, A. A. *J. Am. Chem. Soc.* **1992**, *114*, 5439.

(9) (a) Chen, C.-H.; Vesecky, S. M.; Gewirth, A. A. *J. Am. Chem. Soc.* **1992**, *114*, 451. (b) Chen, C.-H.; Gewirth, A. A. *Phys. Rev. Lett.* **1992**, *68*, 1571.

(10) Adzic, R. R. In *Advances in Electrochemistry and Electrochemical Engineering*; Gerischer, H., Tobias, C. W., Eds.; Wiley-Interscience: New York, 1984; Vol. 13, pp 159–260.

(11) Markovic, N. M.; Adzic, R. R. *J. Electroanal. Chem.* **1984**, *163*, 437.

(12) Amadelli, R.; Markovic, N.; Adzic, R.; Yeager, E. *J. Electroanal. Chem.* **1983**, *159*, 391.

(13) Polewska, W.; Wang, J.; Ocko, B. M.; Adzic, R. R. *J. Electroanal. Chem.*, in press.

(14) Wang, J.; Ocko, B. M.; Davenport, A. J.; Isaacs, H. *Phys. Rev. B* **1992**, *46*, 10321.

(15) Pourbaix, M. In *Atlas of Electrochemical Equilibria in Aqueous Solutions*; NACE: Cebelcor, 1960; p 445.

(16) Adzic, R. R. In *Modern Aspects of Electrochemistry*; White, R. E., Bockris, J. O'M., Conway, B. E., Eds.; Plenum: New York, 1990; Vol. 21, pp 163–236.

(17) Ocko, B. M.; Watson, G. M.; Wang, J. *J. Phys. Chem.* **1994**, *98*, 897.

(18) The average Tl–Tl spacing of 3.432 Å is calculated by setting the volume of the hcp unit cell for hypothetical fcc cell, which has a unique near-neighbor spacing.

(19) Toney, M. F. Private communication.

(20) (a) Novaco, A. D.; McTague, J. P. *Phys. Rev. Lett.* **1977**, *38*, 1286. (b) McTague, J. P.; Novaco, A. D. *Phys. Rev. B* **1979**, *19*, 5299.

(21) (a) Nielsen, M.; McTague, J. D.; Passell, L. In *Phase Transitions in Surface Films*; Dash, J. D., Ruvalds, J., Eds.; Plenum: New York, 1980; p 127. (b) Cui, J.; Fain, S. C. *Phys. Rev. B* **1989**, *39*, 8628. D'Amico, K. L.; Bohr, J.; Moncton, D. E.; Gibbs, D. *Phys. Rev. B* **1990**, *41*, 4368.

(22) Schultze, J. W.; Vetter, K. J. *J. Electroanal. Chem.* **1973**, *44*, 63.

(23) Adzic, R. R.; Wang, J.; Polewska, W.; Ocko, B. M. *Electrochim. Acta*, in press.

(24) Ocko, B. M.; Wang, J. In *Synchrotron Techniques in Interfacial Electrochemistry*; Melendres, C. A., Tadjeddine, A., Eds.; Kluwer Academic Publishers: Boston, Vol. 432, pp 127–155.

(25) Gibbs, D.; Ocko, B. M.; Zehner, D. M.; Mochrie, S. G. *Phys. Rev. B* **1988**, *38*, 7303.

(26) On the basis of previous reflectivity measurements on Au(111) in NaF solution (ref 14), we have argued that a layer of water molecules may be ordered along the surface normal direction. However, the effect of such a water layer is minimal for high-electron density adlayers as demonstrated previously (refs 5 and 17). Therefore, such a water layer is not included in this model.